Pathophysiology of Dyt1 dystonia is mediated by spinal cord dysfunction

Authors: Amanda M. Pocratsky[1*], [†]Filipe Nascimento[1], [†]M. Görkem Özyurt[1], Ian J. White[3], Roisin Sullivan[4], Calvin C. Smith[1], Sunaina Surana[1,5], Marco Beato[2], Robert M. Brownstone[1*]

Affiliations:

[1]Department of Neuromuscular Diseases, Institute of Neurology, University College London; London, WC1N 3BG, UK.

[2]Department of Neuroscience, Physiology, and Pharmacology, University College London; London, WC1E 6BT, UK.

[3]Electron Microscopy Laboratory, MRC Laboratory for Molecular Cell Biology, University College London; London, WC1E 6BT, UK.

[4]Department of Molecular Neuroscience, Institute of Neurology, University College London; London, WC1N 3BG, UK.

[5]UK Dementia Research Institute, University College London; London, WC1E 6BT, UK.

[†]These authors contributed equally to this work.

*Corresponding authors. Email: a.pocratsky@ucl.ac.uk, r.brownstone@ucl.ac.uk

Abstract:

Dystonia, a neurological disorder defined by abnormal postures and disorganised movements, is thought to be a neural circuit disorder with dysfunction arising within and between multiple brain regions. Given that spinal circuits are the *de facto* final common pathway for motor control, we sought to determine their contribution to the movement disorder. We confined a dystonia-related mutation to the spinal cord, which led to behavioural and physiological recapitulation of a severe form of inherited, early-onset, generalised dystonia. These data challenge our current understanding of dystonia, and lead to broader insights into spinal cord function and its involvement in movement disorder pathophysiology.

One sentence summary:

Spinal *Tor1a* deletion causes severe early onset generalised dystonia, exposing spinal circuitopathy as a key factor in its pathophysiology.

Dystonia is a movement disorder characterised by involuntary sustained muscle contractions leading to spasms, abnormal posturing, and sometimes tremor, which together manifest as disorganised movement. Underlying the abnormal postures and disordered movements is irregular muscle activity that bears 3 main neurophysiological biosignatures: (a) spontaneous muscle contraction at rest (*1*); (b) excessive, sustained contractions during voluntary movements, often resulting in painful co-contractions of antagonistic muscles (*1*, *2*); and (c) altered involuntary sensory-motor reflexes (*3*, *4*). Dystonia can be acquired or inherited, with the most prevalent genetic form being early onset, generalised DYT1-*TOR1A* dystonia, caused most commonly by an in-frame deletion of 3 base pairs in exon 5 of the TorsinA (*TOR1A*) gene (*5*).

As dystonia is a movement disorder, clinical and fundamental research has primarily focused on dysfunction within the basal ganglia: a cluster of nuclei that play a role in movement selection and are core sites of pathology in other movement disorders such as Parkinson's disease and Huntington's disease (*6*, *7*). In dystonia, however, there is limited pathology in the basal ganglia (*8*), a multi-month lag between acquired injury of the nuclei and development of dystonia (*9*), and a similar lag between treatment of dystonia with deep brain stimulation and ameloration of symptoms (*10*). Moreover, not all basal ganglia lesions give rise to dystonia (*7*). Hence dystonia is now commonly considered to be a circuitopathy comprising multiple brain regions involved in movement, including the basal ganglia, thalamus, cerebellum, and cortex (*6*).

Given that the spinal cord is the final common pathway for motor control, contains multi-layered neuronal circuits that dynamically shape and organise motor output (*11*), that the face is rarely affected in DYT1-*TOR1A* dystonia (*12*), and that dystonia is defined by its movement disorganisation (*1*), we sought to determine whether the spinal cord could be responsible for the pathogenesis of the clinical signs of dystonia. To do so, we made a mouse model of DYT1-*TOR1A* dystonia that limits *Tor1a* knockout to spinal cord neurons. We show that these mice develop behavioural and physiological signs that mirror those in human DYT1-*TOR1A* dystonia, and correspondingly have spinal circuit dysfunction. We conclude that spinal-restricted knockout of *Tor1a* reproduces the pathophysiology of the human condition. These findings also highlight the key role that the spinal cord plays in organising movement, and the importance of considering spinal circuits in the pathophysiology of movement disorders.

Results

Restricting *Tor1a* deletion to spinal circuits

Unravelling the specific contributions of spinal cord dysfunction to movement disorganisation in Dyt1-*Tor1a* dystonia requires site specificity in *Tor1a* deletion: that is, spinal circuits must be directly affected while supraspinal centres are spared. To this end, we used the established Cdx2::FlpO transgenic mouse model as our genetic entry point to manipulating *Tor1a* in spinal circuits as flippase expression is restricted to the developing spinal cord (*13*). Drawing inspiration from a prevailing Tor1a-flox approach (*14-16*), we developed a new Tor1a-frt mouse in which exons 3-5 are flanked by frt sites (Fig. 1A; Fig. S1A). Through multigenerational breeding of Tor1a-frt with spinal-targeting Cdx2::FlpO mice, we generated a spinal-restricted biallelic "double" conditional knockout (d-cko) of *Tor1a* (Fig. S1B). Probing for *Tor1a* and torsinA protein expression in brains and lumbar spinal cords confirmed the site-specificity of this approach. When compared to FlpO-negative littermate controls (Cdx2::wt;Tor1a$^{frt/frt}$), spinal *Tor1a* d-cko (Cdx2::FlpO;Tor1a$^{frt/frt}$) mice showed normal *Tor1a*-torsinA expression in brain, but a significant reduction in lumbar spinal cords (Fig. 1B-C), thus validating the site-specificity of our strategy.

Nuclear envelope pathology in *Tor1a*-deleted spinal neurons

We next screened for anatomical biosignatures of torsinA dysfunction: nuclear envelope (NE) malformations. Canonical torsinA expression in neurons is distributed throughout the endoplasmic reticulum and NE, but in loss-of-function mutations, torsinA aberrantly accumulates in the NE (*17*). Morphologically, this can lead to outer nuclear membrane protrusions that balloon into the perinuclear space where they are released as vesicles (*15, 18, 19*). We found that, while littermate control spinal neurons had normal, well-defined, closely-apposed nuclear bilayers with occasional nucleoplasmic reticulations decorating the nuclei (Fig. 1D-F, J-K, arrowhead), *Tor1a*-deleted lumbar spinal neurons were chockfull of NE abnormalities. In the dorsal horn, there were groups of spinal neurons that appeared normal (Fig. 1G), exhibited early signs of NE budding with sparse vesicle accumulation (Fig. 1H), or showed vesicle-packed perinuclear space with overt separation of the nuclear membranes (Fig. 1I). In the ventral horn, almost all spinal neurons screened were affected, with the perinuclear space filled with NE-derived vesicles (Fig. 1L). Multiple vesicles often budded from one protrusion point of the inner nuclear membrane (Fig. 1M) with signs of

electron-dense chromatin content filling the vesicles and being released (Fig. 1N). Large area ultrastructural analysis via backscatter scanning electron microscopy of all contiguous spinal neurons embedded within hemicord slices corroborated the ventro-dorsal gradient in NE severity (available at open access data repository). Of note, transmission ultrastructural screening of basal ganglia neurons - the historical epicentre of dystonia pathogenesis - did not show aberrant NE budding or vesiculation (Fig. S2). Together, these data confirm that this new model confines the *Tor1a* d-cko to spinal neurons, which manifest anatomical biosignatures of torsinA loss-of-function.

Spinal-restricted *Tor1a* leads to severe early-onset, generalised dystonia

Severe DYT1-*TOR1A* is defined by a core set of clinical features; most salient are the eponymizing motor symptoms: early onset, generalised spread of disorganised movements (*20*). Motor dysfunction emerges early in infancy to childhood, usually at a lower extremity (*20*). Over time, motor signs generalise, spreading rostrally to the trunk and upper limbs, stabilizing at or below the neck, usually sparing cranial muscle function (*11*). We discovered a striking similarity between severe DYT1-*TOR1A* and spinal *Tor1a* d-cko mice (Fig. 2A-H). The motor impairments emerged early, within the first 1-3 days post-birth, manifesting caudally as hindlimb hyperextension (Fig. 2A; Movie S1). These signs spread bilaterally to affect both lower extremities by postnatal day 5 (Fig. 2B). With increasing age the motor impairments spread rostrally such that by postnatal day 7-9 there were clear signs of pelvis, trunk, and forelimb dysfunction, with the forelimbs abnormally extended forward and minimal body weight support (Fig. 2C-D). By postnatal day 11, the motor signs became fixed at or below the head, sparing orofacial movements. Stepping was impaired as indicated by excessive hindlimb hyperextension with minimal flexion (Fig. 2E). Hindpaw clasping and truncal torsion occurred during tail suspension (Fig. 2F; Movie S2), a test commonly used in Dyt1-*Tor1a* dystonia animal models to uncover latent dystonic-like behaviours (*21*, *22*). By postnatal day 19-21, spinal *Tor1a* d-cko mice were severely dystonic with profound disorganisation of limb movements during voluntary behaviour (Fig. 2G; Movie S3), with interrupting bouts of debilitating truncal torsion (Fig. 2H; Movie S4). Similar to severe DYT1-*TOR1A*, postures were abnormal (Movie S5) and movements were disorganised, jerky, and tremulous in spinal *Tor1a* d-cko mice (Movie S6).

After establishing that spinal-restricted *Tor1a* d-cko causes an early-onset, generalised movement disorder, we set out to unambiguously define the spatiotemporal window of the dystonic-like phenotype. Five external raters experienced with mouse behaviour were recruited to provide unbiased analyses of postnatal sensory-motor development in littermate controls vs spinal *Tor1a* d-cko mice (Fig. 2I), all while blinded to the study design, disease model, mutation, and anticipated motor impairments. Raters assessed postnatal video recordings (postnatal day 1-13) and selected - via a unidirectional online test - whether the mouse was a "control" or "mutant," the latter prompting a follow-up question to select the body region(s) affected. The unbiased external analysis corroborated our internal findings. At postnatal day 1, the accuracy rate (proportion of correct observations) in the unbiased detection of spinal *Tor1a* d-cko mice was >60% (Fig. 2J). Throughout postnatal maturation, the accuracy rate steadily increased until it reached 100% at postnatal day 7 with any subsequent inaccuracy due to false positives (Fig. S3A; P1-P6: 73% sensitivity, 88% specificity; P7-P13: 100% sensitivity, 98% specificity). A clear spatiotemporal pattern emerged from these unbiased assessments, with motor impairments noted early in the hindlimbs, then spreading rostrally to affect the pelvis, trunk, and forelimbs, with the head minimally affected (Fig. 2K; Fig. S3B-G). Thus, *Tor1a* dysfunction confined to spinal circuits causes an overt movement disorder that recapitulates the spatiotemporal motor symptoms of severe early-onset, generalised dystonia.

The disordered postures and movements observed in severe DYT1-*TOR1A* are defined by two biosignatures within the underlying muscle activity: (a) persistent involuntary electromyogram (EMG) activity at rest (*1*) and (b) disorganised muscle activity during voluntary movements, often including antagonistic co-contractions (*1, 2*). Leveraging the limited mobility observed in spinal *Tor1a* d-cko mice, we performed acute EMG recordings from the antagonistic tibialis anterior (Ta) and gastrocnemius (G) hindlimb muscles to measure muscle activity at rest, during tail suspension, and during voluntary locomotor movements (Fig. 2L). Similar to severe DYT1-*TOR1A*, spinal *Tor1a* d-cko mice show excessive, spontaneous activity at rest, including prolonged co-contraction bursting in antagonist muscles (Fig. 2M; Fig. S4F-G), with few periods of quiescence (Fig. S4A-B). This activity was replete with single unit spikes coincident in the flexor and extensor antagonists (Fig. 2M; Fig. S4D-E). We also noted the intrusion of rhythmic co-contractions, which manifested as a tremulous-like phenotype while animals were at rest (Fig. S4H-O), a phenomenon also reported in dystonia patients (*2*). Tail suspension uncovered a spectrum of EMG patterns

ranging from alternation between flexor-extensor bursting to large amplitude co-contractions (Fig. 2N; Fig. S4R-S), and burst disorganisation between Ta-G that was interspersed with tonic activity and rhythmic co-contractions (Fig. S4T-U). During volitional stepping, spinal *Tor1a* d-cko mice showed abnormal hindlimb muscle activity with multiple bouts of antagonistic co-contractions (Fig. 2O; Fig. S4R-S). In total, Ta-G co-contractions accounted for over one-third of the bursting activity observed (Fig. 2P) with intra-animal analysis revealing that Ta-G co-contraction was the dominant bursting pattern observed in half of the cohort (Fig. S4V). This is clearly an underestimate of the amount of co-activity: when considering single unit coincident activity in addition to the bursts, the proportion of co-contraction time increased (Fig. S4W-X). Disorganised hindlimb muscle activity was underscored by a considerable range in frequency and duration of bursts (Fig. S4Y-Z). Together, these data reveal that spinal-restricted *Tor1a* dysfunction directly leads to an early-onset, generalised dystonic-like movement disorder defined by persistent spontaneous muscle activity at rest and excessive co-contractions during voluntary movements.

Excessive, disorganised motor output in spinal *Tor1a*-deleted mice

The similarity between severe DYT1-*TOR1A* and spinal *Tor1a* d-cko mice raised a fundamental question: are *Tor1a*-deleted spinal circuits the principal source of excessive spontaneous activity and disorganised motor output? Given that the lower extremities are a primary site for disease onset in severe DYT1-*TOR1A* and spinal *Tor1a* d-cko mice, we performed targeted recordings of neural activity intrinsic to the lumbar enlargement - the neural hub for hindlimb motor control (*12*). Lumbar spinal cords were isolated from postnatal day 1-5 mice, thus eliminating the influence of descending systems on spinal motor output and framing the previously-defined window of emerging hindlimb dysfunction. Extracellular electrodes were attached to the caudal and rostral lumbar ventral roots to record electroneurogram (ENG) activity from extensor- and flexor-related spinal motor pools, respectively, during “rest” and during drug-induced fictive locomotion (*23*).

In early postnatal isolated spinal cords, there is often spontaneous ENG activity at rest, a transient phenomenon that dissipates until little - if any - unevoked activity is present by postnatal day 4-5 (*24*), as seen in our littermate controls (Fig. 3B). Spinal *Tor1a* d-cko mice, on the other hand, showed excessive spontaneous ENG activity, including extensive antagonistic co-activation of

caudal extensor-related (L5) and rostral flexor-related (L2) motor pools (Fig. 3C-D). These results show that the spontaneous activity seen in the EMGs *in vivo* can be accounted for by activity in the spinal cord circuits.

Spinal circuits can directly organise and produce rhythmic, coordinated output from flexor-extensor motor pools that manifests as the intra- and interlimb movements defining locomotion (*12*). These circuits can be activated *in vitro* by application of neurotransmitters to produce a correlate of *in vivo* locomotion, called fictive locomotion. In littermate controls during fictive locomotion, there is stable rhythmic alternation between bilateral flexor-related (rostral lumbar segments, L2), bilateral extensor-related (caudal lumbar segments, L5), and ipsilateral flexor-extensor related ventral roots (Fig. 3D). In the first 24 hours post-birth, apart from select instances where the normally alternating flexor-extensor activity drifts to synchrony (Fig. 2E, vertical line), spinal motor output in *Tor1a*-deleted mice is largely similar to littermate controls (Fig. S5). But by postnatal day 2, the previously normal alternating flexor-extensor bursting activity becomes disorganised (Fig. 2F; Fig. S5), with prolonged bursting at the caudal extensor-related lumbar motor pools, variable burst durations in the rostral flexor-related motor pools, and co-activation between the flexor- and extensor-related spinal motor pools. By postnatal day 4, ENG bursting was profoundly altered across the lumbar spinal cord (Fig. 3G).

Neural oscillations can be defined by their power, frequency, and phase relationship over time. To determine how the spinal *Tor1a* d-cko fundamentally alters neural output, tiered wavelet transformations were used (*25*). We first isolated the dominant power-frequency bands and cycle durations at individual roots (Fig. S5A-E). We then proceeded with a set of cross-root wavelet transformations to extract the shared power, burst frequency, cycle duration, and phase relationships that define: (a) left-right extensor-related (bilateral caudal roots, L4-L5), (b) left-right flexor-related (bilateral rostral, L1-L2), and (c) ipsilateral flexor-extensor related neural activity. The resultant cross-root convolutions were plotted (Fig. 3H-L) and the dominant (high-power) cross-root burst frequency, cycle duration (Fig. S5), and phase relationships over time were extracted for quantitative analysis of spinal motor output.

Littermate controls showed a consistent dominant high-power frequency band confined to 0.125-0.50 Hz for each root pair assessed (Fig. 3H,L). This power-frequency profile was also observed

in spinal *Tor1a* d-cko mice at postnatal day 1 (Fig. 3I). But by postnatal day 3 (Fig. 3J), spinal *Tor1a* d-cko mice showed a clear disruption to the signal power-frequency spectrum with a downward shift in burst frequency such that by postnatal day 5, the dominant power-frequency band was ~0.016 Hz (Fig. 3K). Extracting the shared frequencies from the high-power bands revealed a significant decrease in drug-induced burst frequency in all root pairs assessed (Fig. 3M-O). This decrease in burst frequency translated to a ~4-5-fold increase in the cross-root burst cycle duration (Fig. S5F-H).

After establishing the *Tor1a* cko-induced changes to the power-frequency profile, we shifted our focus to cross-root burst coordination, a correlate of the disorganised movements that affect people with dystonia. Cross-root burst coordination data were extracted from the dominant power-frequency bands and plotted on circular graphs wherein 0° denotes in-phase synchrony and 180° reflects out-of-phase alternation.

The classic locomotor profile of out-of-phase bursting activity between bilateral extensors, bilateral flexors, and ipsilateral flexor-extensors was observed in the littermate controls, with phase data concentrated at 180° (Fig. 3P-R) (*12*). For the most part, the burst coordination observed in postnatal day 1 spinal *Tor1a* d-cko mice was broadly similar to littermate controls (Fig. S5L). However, this normal bursting profile became disrupted at postnatal day 2-5 wherein there was a predominant shift in the bursting activity towards in-phase synchrony (Fig. 3P-R). Cross-root coherence remained above 0.8 for all root pairs examined (Fig. S5I-K), suggesting that disruption to rhythmic bursting observed in one root was largely related or predictive of the disrupted bursting activity observed in the other root. Together, these data reveal that *Tor1a*-deleted spinal circuits directly produce excessive spontaneous activity at rest and disorganised motor output during locomotion.

Spinal monosynaptic reflexes are impaired in spinal *Tor1a* conditional knockouts

Given the spinal locomotor circuit dysfunction, we next looked at the most basic spinal circuit, one that can also be readily studied in humans: the monosynaptic (myotatic) reflex. Case reports indicate that individuals with generalised dystonia, including genetically-confirmed DYT1-*TOR1A*, show diminished monosynaptic reflex amplitudes (*3, 26*), increased variability in the evoked response amplitude (*3, 4*), and the infiltration of aberrant asynchronous activity (*3*). We

thus systematically assessed the monosynaptic reflex across space (L1-L5) and time (P7-P13, an age range where the phenotype is fully penetrant) in spinal *Tor1a* d-cko mice.

Graded stimuli were applied to the dorsal root and the evoked monosynaptic reflex was recorded from the ventral root (Fig. 4A, bottom). Plotting representative monosynaptic reflexes revealed a spatiotemporal pattern parallel to the dystonic-like phenotype. Compared to age-matched littermate controls, *Tor1a* d-cko spinal reflexes were reduced in the caudal-most root at postnatal day 7, but otherwise broadly normal in the rostral roots (L1, L3) (Fig. 4B). With increasing postnatal age, the impairments to the monosynaptic spinal reflex spread rostrally, affecting L3 and L1 by postnatal day 11-13. Closer examination of the constituent components of the reflex response (Fig. 4C) revealed that the reflexes in spinal-restricted *Tor1a* d-cko mice had lower amplitudes (Fig. S6G) and longer durations (Fig. 4C-D), with multiple asynchronous peaks (Fig. S6A-F; Fig. S6H). In addition to impairments in the reflex response itself, the latency to onset - a measure largely dependent on afferent conduction - was significantly increased in spinal *Tor1a* d-cko mice compared to littermate controls (Fig. 4G-I; Fig. S6I). Together, these data suggest that there is a clear caudal-to-rostral progression in monosynaptic spinal reflex impairments during postnatal maturation, with a dispersion of the reflex across time.

Spinal *Tor1a* deletion leads to distributed pathophysiology in the monosynaptic reflex

We next sought to gain mechanistic insights into reflex dysfunction by interrogating the four constituent components of this reflex arc: (a) proprioceptive afferents in the dorsal roots, (b) synapses with motoneurons, (c) the motoneurons themselves, and (d) efferent transmission in the ventral root. We focused on the caudal lumbar motor pools (L4-L5) as they are the earliest affected. We used a ventral horn ablated preparation (Fig. 5A, left) to determine whether motoneurons were intrinsically affected by the spinal-restricted *Tor1a* deletion. Motoneurons in spinal *Tor1a* d-cko mice appeared smaller than those in littermate controls (Fig. 5B). While spinal *Tor1a* d-cko motoneurons had similar resting membrane potentials as control motoneurons (Fig. 5C), there was a significant reduction in whole cell capacitance (Fig. 5D) and a ~350% increase in input resistance (Fig. 5E), consistent with the smaller cell size. Together, these data indicate that lumbar motoneurons are directly affected by *Tor1a* deletion.

But smaller motoneurons alone could not explain all the changes in the monosynaptic reflex, so we next focussed on the afferent limb of the reflex using low-threshold stimulation of the dorsal roots. Compared to littermate controls, spinal *Tor1a* d-cko afferent-evoked excitatory post-synaptic currents (EPSCs) had reduced amplitude, prolonged duration, and multiple asynchronous peaks (Fig. 5F) - outcomes that were corroborated when we activated a subset of afferent fibres via discrete microstimulations (Fig. S7C-D). At all ages assessed, the EPSC area - a measure of charge carried - was decreased in spinal *Tor1a* d-cko motoneurons compared to controls (Fig. 5G; Fig. S7A). There was a decrease in EPSC conductance (Fig. 5H), but when scaled to input conductance there was no difference (Fig. 5I), suggesting that monosynaptic input was more or less normal for the motoneuron sizes. Of note, at all ages tested, there was a significant increase in the latency to dorsal root-evoked monosynaptic EPSC in spinal *Tor1a* d-cko mice as compared to controls (Fig. 5J; Fig. S7B), a finding that parallels the increased latencies observed in extracellular recordings.

While the longer latencies could result from impairments at the Ia-motoneuron synapse, they could also simply be due to deficits in afferent conduction itself. Thus, we recorded L4 and L5 dorsal root volleys in response to root stimulation (Fig. 5K), and found slower afferent conduction velocities in spinal *Tor1a* d-cko mice compared to controls (Fig. 5L-M), suggesting that the longer latencies to EPSCs resulted from slower conduction velocities. But increased latencies alone cannot account for the asynchronous peaks observed in EPSCs. To this end, we microstimulated the dorsal roots at various sites, activating small subsets of fibres (Fig. 5N-O). After scaling the conduction time by distance, we discovered that spinal *Tor1a* d-cko mice showed longer and variable conduction times as compared to controls (Fig. 5P), suggesting that the multiple peaks in the EPSCs result from time dispersion of the incoming afferent action potentials. That is, two effects occur in the dorsal roots of the spinal *Tor1a* d-cko mice: slower conduction velocities and increased variance of these velocities across fibres.

Given the conduction impairments in dorsal roots, we turned to the ventral roots to determine whether motor axons are also affected (Fig. S7E). We found a modest, but significant decrease in efferent conduction velocity in spinal *Tor1a* d-cko mice as compared to controls (Fig. S7F-G). Responses to microstimulation also revealed increased scaled conduction times and variances in the ventral roots (Fig. S7H-I). In summary, all compartments of the monosynaptic reflex arc - from

action potential conduction of sensory afferents to motoneurons to efferent output in the motor roots themselves - are vulnerable to *Tor1a* dysfunction and contribute to impaired sensory-motor integration in *Tor1a* d-cko mice.

Discussion

We have uncovered that spinal circuit dysfunction is a key contributor to the pathophysiology of DYT1-*TOR1A* dystonia. To unambiguously test our hypothesis, we confined a biallelic conditional knockout of *Tor1a* confined to the spinal cord, leaving its expression intact throughout the rest of the nervous system. These mice had the hallmarks of DYT1-*TOR1A*: (a) spontaneous muscle contractions at rest (*1*); (b) excessive, sustained contractions during voluntary movements (*1, 2*); and (c) altered sensory-motor reflexes (*3, 4*).

Given that the spinal cord is comprised of neural circuits that control the basic "syllables" of movement (*27*), and the motor signs of dystonia result from abnormal control of these fundamental components of movement, there was clear logic in considering that spinal circuit dysfunction leads to the signs of DYT1-*TOR1A*. In fact, there are seeds of substantiation sprinkled through the literature that point to spinal circuit dysfunction. For example, Dyt1-*Tor1a* animal studies have shown nuclear envelope malformations in spinal neurons (*15, 18*), spinal motoneuron loss (*14*), and reduced spinal GABAergic inputs onto primary afferent fibres (*28*). In non-Dyt1 dystonia models, *Lamb1t* mice have coincident EMG activity between opposing muscles, a phenomenon that persists post-spinal transection and thus directly implicates dysfunctional spinal circuits (*29*). And in people affected by DYT1-*TOR1A*, analyses of spinal reflexes indicate that dystonic individuals have impairments in monosynaptic stretch reflexes (*3, 4*) and reciprocal inhibition that serves to prevent co-activation of antagonists (*1, 30-32*). Even though these reflexes are mediated by spinal circuits, the impairments observed have been attributed to dysfunction of descending systems (*30, 33*). But spinal circuits are complex, and form specialised, multi-layered networks that integrate supraspinal, spinal, and sensory inputs to organise motor output (*34*). These circuits are multi-functional and flexible, producing a broad range of motor patterns (*35*) with the intrinsic capacity for dynamic reconfiguration (*36*). Thus, in dystonia pathophysiology, spinal circuits are likely a critical nexus for neurological dysfunction and movement disorganisation.

Dystonia is clearly a circuitopathy, and as such should be considered as a process that affects motor circuits throughout the central nervous system. Disease processes (e.g. basal ganglia stroke) or treatments (e.g. pallidal deep brain stimulation) targeting one portion of these circuits may, after many months, lead to or alleviate dystonia, respectively (*9*, *10*), presumably through changes involving remote circuits. But one way or another - directly or indirectly - new treatments will need to address the pathophysiology underlying symptoms, the circuits of which are largely resident in the spinal cord.

References and Notes:

1. J. C. Rothwell, J. A. Obeso, B. L. Day, C. D. Marsden, Pathophysiology of dystonias. *Advances in neurology* **39**, 851-863 (1983).
2. L. G. Cohen, M. Hallett, Hand cramps: clinical features and electromyographic patterns in a focal dystonia. *Neurology* **38**, 1005-1012 (1988). doi: 10.1212/wnl.38.7.1005
3. V. P. Novikova, Spinal mechanisms of motor disturbances in torsion dystonia (an electromyographic analysis). *Neurosci Behav Physiol* **11**, 353-357 (1981). doi: 10.1007/BF01184199
4. J. H. Koelman et al., Soleus H-reflex tests in dystonia. *Movement disorders: official journal of the Movement Disorder Society* **10**, 44-50 (1995). doi: 10.1002/mds.870100109
5. L. J. Ozelius et al., The TOR1A (DYT1) gene family and its role in early onset torsion dystonia. *Genomics* **62**, 377-384 (1999). doi: 10.1006/geno.1999.6039
6. H. A. Jinnah, V. Neychev, E. J. Hess, The Anatomical Basis for Dystonia: The Motor Network Model. *Tremor and other hyperkinetic movements* **7**, 506-506 (2017). doi: 10.7916/D8V69X3S
7. V. K. Neychev, R. E. Gross, S. Lehéricy, E. J. Hess, H. A. Jinnah, The functional neuroanatomy of dystonia. *Neurobiology of disease* **42**, 185-201 (2011). doi: 10.1016/j.nbd.2011.01.026
8. R. Paudel, J. Hardy, T. Revesz, J. L. Holton, H. Houlden, Review: Genetics and neuropathology of primary pure dystonia. *Neuropathol Appl Neurobiol* **38**, 520-534 (2012).
9. B. L. Scott, J. Jankovic, Delayed-onset progressive movement disorders after static brain lesions. *Neurology* **46**, 68-74 (1996). doi: 10.1111/j.1365-2990.2012.01298.x
10. A. M. Lozano, W. D. Hutchison, S. K. Kalia, What Have We Learned About Movement Disorders from Functional Neurosurgery? *Annual review of neuroscience* **40**, 453-477 (2017). doi: 10.1146/annurev-neuro-070815-013906
11. O. Kiehn, Locomotor circuits in the mammalian spinal cord. *Annual review of neuroscience* **29**, 279-306 (2006). doi: 10.1146/annurev.neuro.29.051605.112910
12. S. B. Bressman et al., Dystonia in Ashkenazi Jews: clinical characterization of a founder mutation. *Ann Neurol* **36**, 771-777 (1994). doi: 10.1002/ana.410360514
13. O. Britz et al., A genetically defined asymmetry underlies the inhibitory control of flexor-extensor locomotor movements. *eLife* **4**, (2015). doi: 10.7554/eLife.04718

14. S. S. Pappas et al., Forebrain deletion of the dystonia protein torsinA causes dystonic-like movements and loss of striatal cholinergic neurons. *eLife* **4**, e08352 (2015). doi: 10.7554/eLife.08352

15. L. M. Tanabe, C. C. Liang, W. T. Dauer, Neuronal Nuclear Membrane Budding Occurs during a Developmental Window Modulated by Torsin Paralogs. *Cell reports* **16**, 3322-3333 (2016). doi: 10.1016/j.celrep.2016.08.044

16. S. S. Pappas et al., A cell autonomous torsinA requirement for cholinergic neuron survival and motor control. *eLife* **7**, (2018). doi: 10.7554/eLife.36691

17. R. E. Goodchild, W. T. Dauer, Mislocalization to the nuclear envelope: an effect of the dystonia-causing torsinA mutation. *Proceedings of the National Academy of Sciences of the United States of America* **101**, 847-852 (2004). doi: 10.1073/pnas.0304375101

18. R. E. Goodchild, C. E. Kim, W. T. Dauer, Loss of the dystonia-associated protein torsinA selectively disrupts the neuronal nuclear envelope. *Neuron* **48**, 923-932 (2005). doi: 10.1016/j.neuron.2005.11.010

19. C. E. Weisheit, W. T. Dauer, A novel conditional knock-in approach defines molecular and circuit effects of the DYT1 dystonia mutation. *Human molecular genetics* **24**, 6459-6472 (2015). doi: 10.1093/hmg/ddv355

20. X. O. Breakefield, C. Kamm, P. I. Hanson, TorsinA: movement at many levels. *Neuron* **31**, 9-12 (2001). doi: 10.1016/s0896-6273(01)00350-6

21. P. Shashidharan et al., Transgenic mouse model of early-onset DYT1 dystonia. *Human molecular genetics* **14**, 125-133 (2004). doi: 10.1093/hmg/ddi012

22. C. C. Liang, L. M. Tanabe, S. Jou, F. Chi, W. T. Dauer, TorsinA hypofunction causes abnormal twisting movements and sensorimotor circuit neurodegeneration. *The Journal of clinical investigation* **124**, 3080-3092 (2014). doi: 10.1172/JCI72830

23. P. J. Whelan, Developmental Aspects of Spinal Locomotor Function: Insights from Using the in vitro Mouse Spinal Cord Preparation. *J Physiol* **553**, 695-706 (2003). doi: 10.1113/jphysiol.2003.046219

24. A. Bonnot, D. Morin, D. Viala, Genesis of spontaneous rhythmic motor patterns in the lumbosacral spinal cord of neonate mouse. *Developmental Brain Research* **108**, 89-99 (1998). doi: 10.1016/s0165-3806(98)00033-9.

25. Y. Mor, A. Lev-Tov, Analysis of rhythmic patterns produced by spinal neural networks. *Journal of neurophysiology* **98**, 2807-2817 (2007). doi: 10.1152/jn.00740.2007

26. R. Paudel et al., Neuropathological features of genetically confirmed DYT1 dystonia: investigating disease-specific inclusions. *Acta Neuropathologica Communications* **2**, 159 (2014). doi: 10.1186/s40478-014-0159-x

27. R. M. Brownstone, Key Steps in the Evolution of Mammalian Movement: A Prolegomenal Essay. *Neuroscience* **450**, 135-141 (2020). doi: 10.1016/j.neuroscience.2020.05.020

28. J. Zhang et al., A Role for Dystonia-Associated Genes in Spinal GABAergic Interneuron Circuitry. *Cell reports* **21**, 666-678 (2017). doi: 10.1016/j.celrep.2017.09.079

29. Y. B. Liu et al., A dystonia-like movement disorder with brain and spinal neuronal defects is caused by mutation of the mouse laminin beta1 subunit, Lamb1. *eLife* **4**, (2015). doi: 10.7554/eLife.11102

30. K. Nakashima et al., Reciprocal inhibition between forearm muscles in patients with writer's cramp and other occupational cramps, symptomatic hemidystonia and hemiparesis due to stroke. *Brain: a journal of neurology* **112**, 681-697 (1989). doi: 10.1093/brain/112.3.681

31. M. Panizza, S. Lelli, J. Nilsson, M. Hallett, H-reflex recovery curve and reciprocal inhibition of H-reflex in different kinds of dystonia. *Neurology* **40**, 824-828 (1990). doi: 10.1212/wnl.40.5.824

32. A. Priori, A. Berardelli, B. Mercuri, M. Manfredi, Physiological effects produced by botulinum toxin treatment of upper limb dystonia. Changes in reciprocal inhibition between forearm muscles. *Brain: a journal of neurology* **118**, 801-807 (1995). doi: 10.1093/brain/118.3.801

33. M. E. Panizza, M. Hallett, J. Nilsson, Reciprocal inhibition in patients with hand cramps. *Neurology* **39**, 85-89 (1989). doi: 10.1212/wnl.39.1.85

34. R. M. Brownstone, T. V. Bui, Spinal interneurons providing input to the final common path during locomotion. *Progress in brain research* **187**, 81-95 (2010). doi: 10.1016/B978-0-444-53613-6.00006-X

35. A. Berkowitz, A. Roberts, S. R. Soffe, Roles for multifunctional and specialized spinal interneurons during motor pattern generation in tadpoles, zebrafish larvae, and turtles. *Front Behav Neurosci* **4**, 36-36 (2010). doi: 10.3389/fnbeh.2010.00036

36. A. M. Pocratsky et al., Long ascending propriospinal neurons provide flexible, context-specific control of interlimb coordination. *eLife* **9**, (2020). doi: 10.7554/eLife.53565

37. C. Welinder, L. Ekblad, Coomassie Staining as Loading Control in Western Blot Analysis. *Journal of Proteome Research* **10**, 1416-1419 (2011). doi: 10.1021/pr1011476

38. T. J. Deerinck *et al.*, Enhancing Serial Block-Face Scanning Electron Microscopy to Enable High Resolution 3-D Nanohistology of Cells and Tissues. *Microscopy and Microanalysis* **16**, 1138-1139 (2010). doi: 10.1017/S1431927610055170

39. W. M. Fox, Reflex-ontogeny and behavioural development of the mouse. *Animal Behaviour* **13**, 234-IN235 (1965). doi: 10.1016/0003-3472(65)90041-2

40. Z. Jiang, K. P. Carlin, R. M. Brownstone, An in vitro functionally mature mouse spinal cord preparation for the study of spinal motor networks. *Brain Research* **816**, 493-499 (1999). doi: 10.1016/s0006-8993(98)01199-8

41. T. V. Bui *et al.*, Circuits for grasping: spinal dI3 interneurons mediate cutaneous control of motor behavior. *Neuron* **78**, 191-204 (2013). doi: 10.1016/j.neuron.2013.02.007

42. M. G. Özyurt, J. Ojeda-Alonso, M. Beato, F. Nascimento, In vitro longitudinal lumbar spinal cord preparations to study sensory and recurrent motor microcircuits of juvenile mice. *bioRxiv*, 2022.2004.2025.489385 (2022). doi: 10.1101/2022.04.25.489385

43. G. P. Dugué, A. Dumoulin, A. Triller, S. Dieudonné, Target-Dependent Use of Coreleased Inhibitory Transmitters at Central Synapses. *J Neurosci* **25**, 6490-6498 (2005). doi: 10.1523/JNEUROSCI.1500-05.2005

44. J. Ho, T. Tumkaya, S. Aryal, H. Choi, A. Claridge-Chang, Moving beyond P values: data analysis with estimation graphics. *Nature Methods* **16**, 565-566 (2019). doi: 10.1038/s41592-019-0470-3

45. A. M. Pocratsky *et al.*, Reversible silencing of lumbar spinal interneurons unmasks a task specific network for securing hindlimb alternation. *Nature communications* **8**, 1963 (2017). doi: 10.1038/s41467-017-02033-x

Acknowledgements:

We are grateful to Nadine Simons-Weidenmaier, Rafaela Fernandez De La Fuente, and Hrista Micheva for assisting in animal husbandry and beta-testing of scoring system; Stuart Martin for initial genotyping and qPCR support; Kim Dougherty (Drexel University), Shayna Singh (Drexel University), Emily Reedich (University of Rhode Island), Cecilia Badenhorst (University of Calgary), and Monica Gorassini (University of Alberta) for serving as our external raters for unbiased phenotyping. We thank Darlene Burke (University of Louisville) for statistical support, Aharon Lev-Tov (Hebrew University of Jerusalem) for providing the SpinalCore software, Martyn Goulding (Salk Institute) for generously providing the Cdx2::FlpO mouse, as well as Tom Warner and Simon Farmer for providing feedback on the manuscript. Thanks to the NVIDIA Corporation for the donation of a Tesla K40 GPU and Quadro RTX 8000.

Funding:

Wellcome Trust Investigator Grant 110193 (RMB)

Medical Research Council Research Grant MR/V003607/1 (RMB) and MR/R011494 (MB and RMB)

Biotechnology and Biological Sciences Research Council Research Grant BB/S005943/1 (MB)

European Molecular Biology Organisation Long Term Fellowship ALTF 495-2018 (AMP)

Sir Henry Wellcome Postdoctoral Fellowship 221610/Z/20/Z (FN)

Royal Society Newton International Fellowship NIF\R1\192316 (MGO)

Human Frontiers Science Program Long Term Fellowship LT000220/2017-L (SS)

Medical Research Council Core Funding Grant MC/U12266B (IW)

Wellcome Trust Facility Grant 218278/Z/19/Z (IW)

Authors contributions:

Conceptualization: RMB, AMP

Methodology: RMB, AMP, MGO & FN & MB (patch clamp recordings and conduction velocity testing), CCS & AMP (*in vivo* electrophysiology), IJW (ultrastructure), RS (qPCR), SS & AMP (Western blots)

Software: AMP, MGO & FN & MB (patch clamp recordings and conduction velocity testing)

Validation: AMP

Formal analysis: AMP, MGO & FN (patch clamp recordings and conduction velocity testing)
Investigation: AMP, MGO & FN (patch clamp recordings and conduction velocity testing), IW (ultrastructure), RS (qPCR), CCS & AMP (*in vivo* electrophysiology), SS & AMP (Western blots)
Resources: RMB, AMP
Data curation: AMP
Writing - original draft: AMP, RMB
Writing - review and editing: RMB, AMP, FN, MGO, MB, CCS, IJW, SS, RS
Visualization: AMP, MGO & FN (patch clamp recordings and conduction velocity testing)
Supervision: RMB
Project administration: RMB
Funding acquisition: RMB (Wellcome, MRC), AMP (EMBO), MB (MRC, BBSRC)

Competing interests:

RMB is a co-founder of Sania Therapeutics, Inc and consults for Sania Rx Ltd.

Data and materials availability:

Data and custom-written code are available at our UCL Research Data Repository entitled "Pocratsky et al 2022" (see methods for access details). The Tor1a-frt mouse model generated in this study is available upon request and/or available through a commercial mouse repository. For the purpose of Open Access, the authors will apply a CC by public copyright licence to the accepted manuscript.

Supplementary materials:

Materials and Methods

Figs. S1 to S7

Table S1

Captions for Movies S1 to S6

Movies S1 to S6

Please refer to the Supplementary Materials document.

Fig. 1

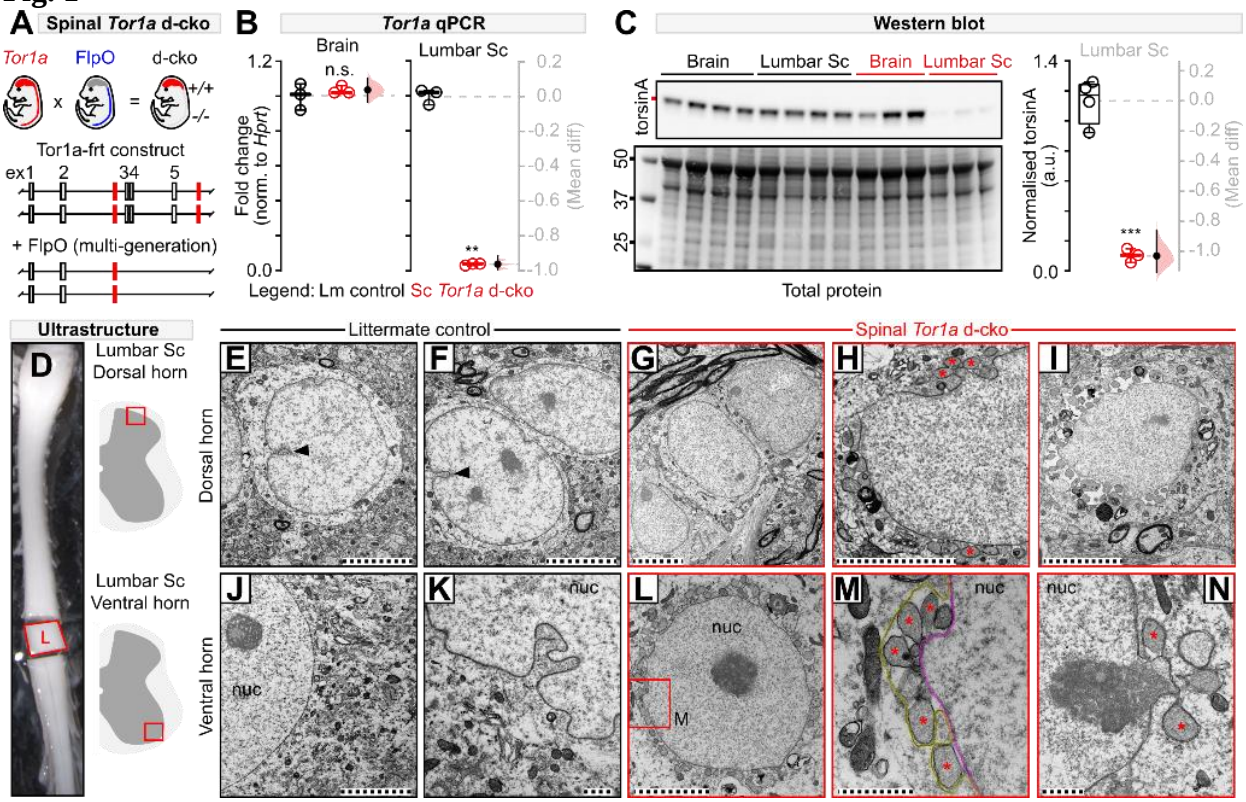

Figure 1. Validation of the spinal-restricted double conditional knockout (d-cko) of *Tor1a*. (**A**) Genetic strategy. (**B**) Unaffected *Tor1a* expression in spinal *Tor1a* d-cko brains (P=0.51, independent t-test; N=3 P18 control, N=3 spinal *Tor1a* d-cko). *Tor1a* expression is absent in lumbar cords of spinal *Tor1a* d-cko (**P<0.001). (**C**) Western blot for torsinA (~37.5 kD) expression in brains and lumbar cords of controls (N=4) and spinal *Tor1a* d-cko (N=3). TorsinA expression is abolished in lumbar cords of P18 spinal *Tor1a* d-cko (***P<0.0001). (**D**) Lumbar cords isolated for ultrastructural analyses of dorsal (**E-I**) and ventral (**J-N**) neurons (P18 N=2 control, N=2 spinal *Tor1a* d-cko). (**E-F**, **J-K**) Control dorsal (**E-F**) and ventral (**J-K**) neurons show normal nuclear membrane morphology with occasional nuclear invaginations (arrowhead). Spinal *Tor1a* d-cko dorsal (**G-I**) and ventral (**L-N**) neurons show NE abnormalities, including perinuclear accumulation of vesicles (asterisk) and separation between the inner (**M**, magenta) and outer nuclear membranes (**M**, yellow). "nuc" = nucleus. Scales: 5µm (E-J, L), 1µm (K, M-N). Group

data shown (box plots) with individual values overlaid (circles) and mean differences (estimation plots). Statistics details in Table S1.

Fig. 2

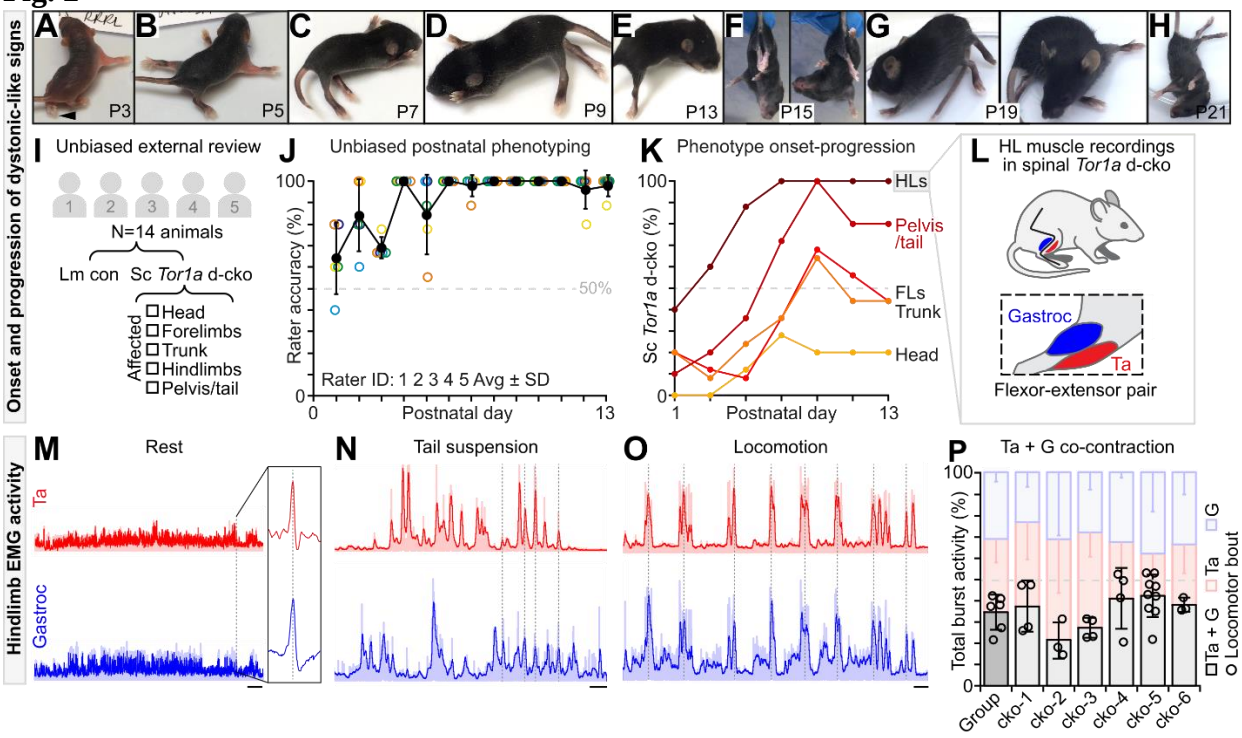

Figure 2. Spinal-restricted *Tor1a* d-cko leads to early-onset, caudo-rostral progression of movement disorganisation marked by abnormal muscle activity. (**A-H**) Onset-progression of dystonic-like signs in spinal *Tor1a* d-cko. (**A**) Signs emerge early (P1-P3) as hindpaw flexion issues (arrowhead) then (**B**) spread rostrally and bilaterally during postnatal maturation leading to hindlimb hyperextension, and (**C-D**) generalise to affect trunk and forelimbs. Affected body regions show (**E**) increased tone, (**F**) hindpaw clasping and trunk torsion, (**G**) abnormal posturing, and (**H**) truncal torsion. (**I**) Experimental design for unbiased external peer review of phenotype (*N*=8 control, *N*=6 spinal *Tor1a* d-cko). (**J**) Rater accuracy. (**K**) Spatiotemporal progression of the spinal *Tor1a* d-cko phenotype. (**L**) EMG recordings from gastrocnemius (G) and tibialis anterior (Ta) (*N*=6 P17-P19 spinal *Tor1a* d-cko). (**M-O**) Linear envelope (dark colours) of rectified EMG activity (light colours) observed (**M**) at rest, (**N**) during tail suspension, and (**O**) locomotion. Vertical lines: co-contraction. (**P**) Co-activation expressed as a proportion of total bursting activity observed during locomotion. "Group": group mean±SD with individual values overlaid (circles).

“cko-1 to -6”: individual mean±SD for total bouts analysed/animal with individual bout values overlaid (circles). Scale: 1s (M), 0.1s (N-O).

514 **Fig. 3**

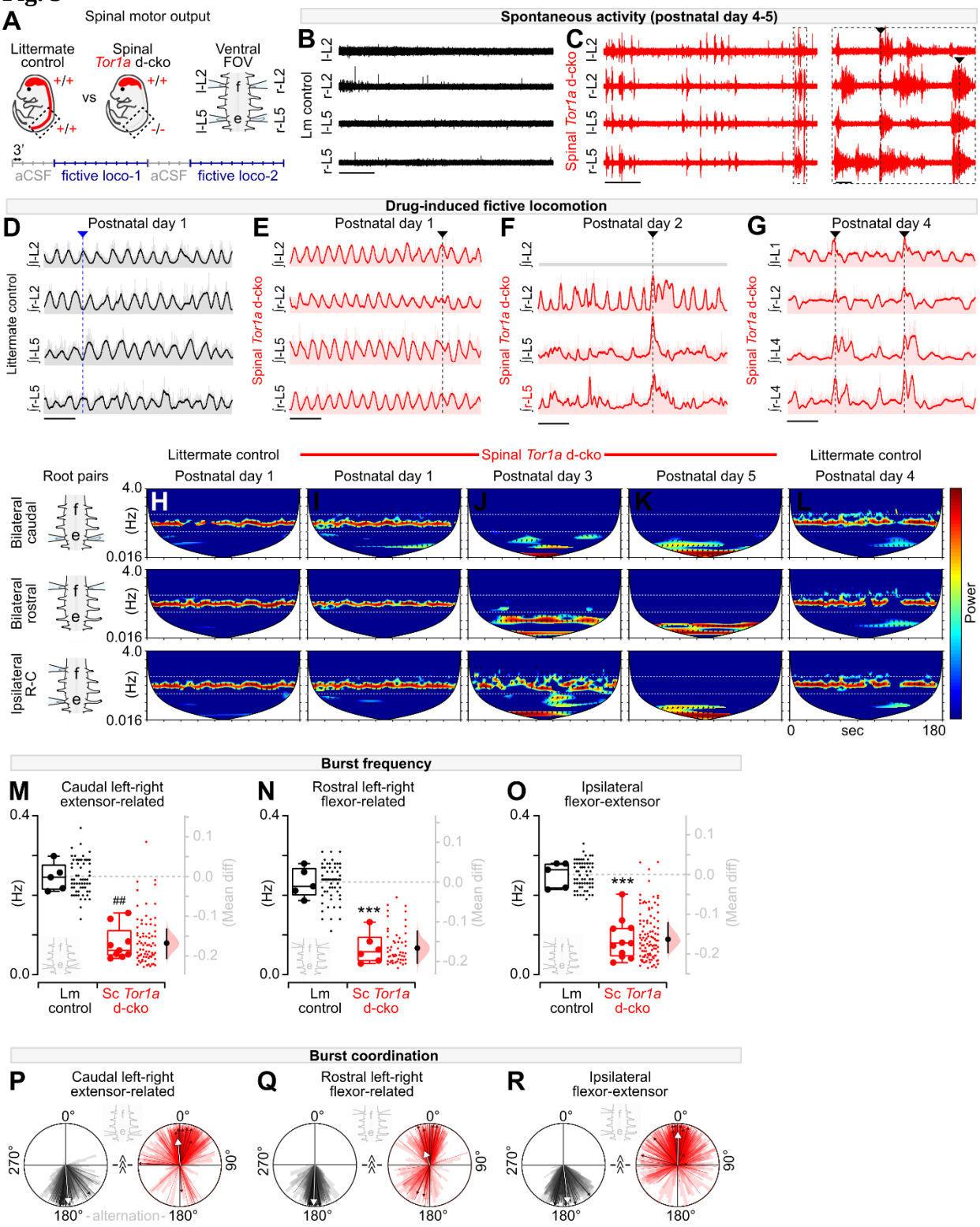
A
Spinal motor output
Littermate control
Spinal Tor1a d-cko
Ventral FOV
vs
+/+
-/-
3'
aCSF
fictive loco-1
aCSF
fictive loco-2
Spontaneous activity (postnatal day 4-5)
B
C
Lm control
Spinal Tor1a d-cko
l-L2
r-L2
l-L5
r-L5
Drug-induced fictive locomotion
D
E
F
G
Postnatal day 1
Postnatal day 2
Postnatal day 4
Littermate control
Spinal Tor1a d-cko
Root pairs
Bilateral caudal
Bilateral rostral
Ipsilateral R-C
Postnatal day 1
Postnatal day 3
Postnatal day 5
Postnatal day 4
H
I
J
K
L
(Hz)
4.0
0.016
Power
0
sec
180
Burst frequency
M
N
O
Caudal left-right extensor-related
Rostral left-right flexor-related
Ipsilateral flexor-extensor
(Hz)
(Mean diff)
##
***
Lm control
Sc Tor1a d-cko
Burst coordination
P
Q
R
0°
90°
180°
270°
alternation

Figure 3. *Tor1a*-deleted spinal circuits produce excessive spontaneous activity and disorganised motor output. (**A**) Experimental design. (**B-C**) Spontaneous activity at "rest" in artificial cerebrospinal fluid (aCSF). (**D**) Rhythmic, coordinated bursting during drug-induced fictive locomotion in control. Dashed line: alternating bursts at L2, L5, and L2-L5. (**E-G**) Drug-induced fictive locomotion in spinal *Tor1a* d-cko. Dashed lines: burst discoordination. (**H-L**) Cross-wavelet analysis of frequency-power (colour, blue-red: 2^7- 2^{13}) spectrum with phase overlaid (arrows). Horizontal lines: control frequency range. (**M-O**) Burst frequency was decreased in all root pairs assessed in spinal *Tor1a* d-cko (N=6-11) vs control (N=5) ($^{\#\#}P$=0.001, Mann-Whitney; ***P<0.0001, independent t-test). Group data shown (box plots) with individual values overlaid (circles) and mean differences (estimation plots). Dots: all epochs analysed/animal. (**P-R**) Burst coordination was affected in all root pairs ($^{\wedge\wedge\wedge}P$<0.001, Watson's non-parametric U^2). Bold arrows, orientation: mean phase, length (0-1): concentration of observations. Group data overlaid onto total observations from all epochs (wedges) and epoch averages (lines). Scale: 30s (B-C, left), 10s, (D-G), 1s (C, right). Statistics details in Table S1.

Fig. 4.

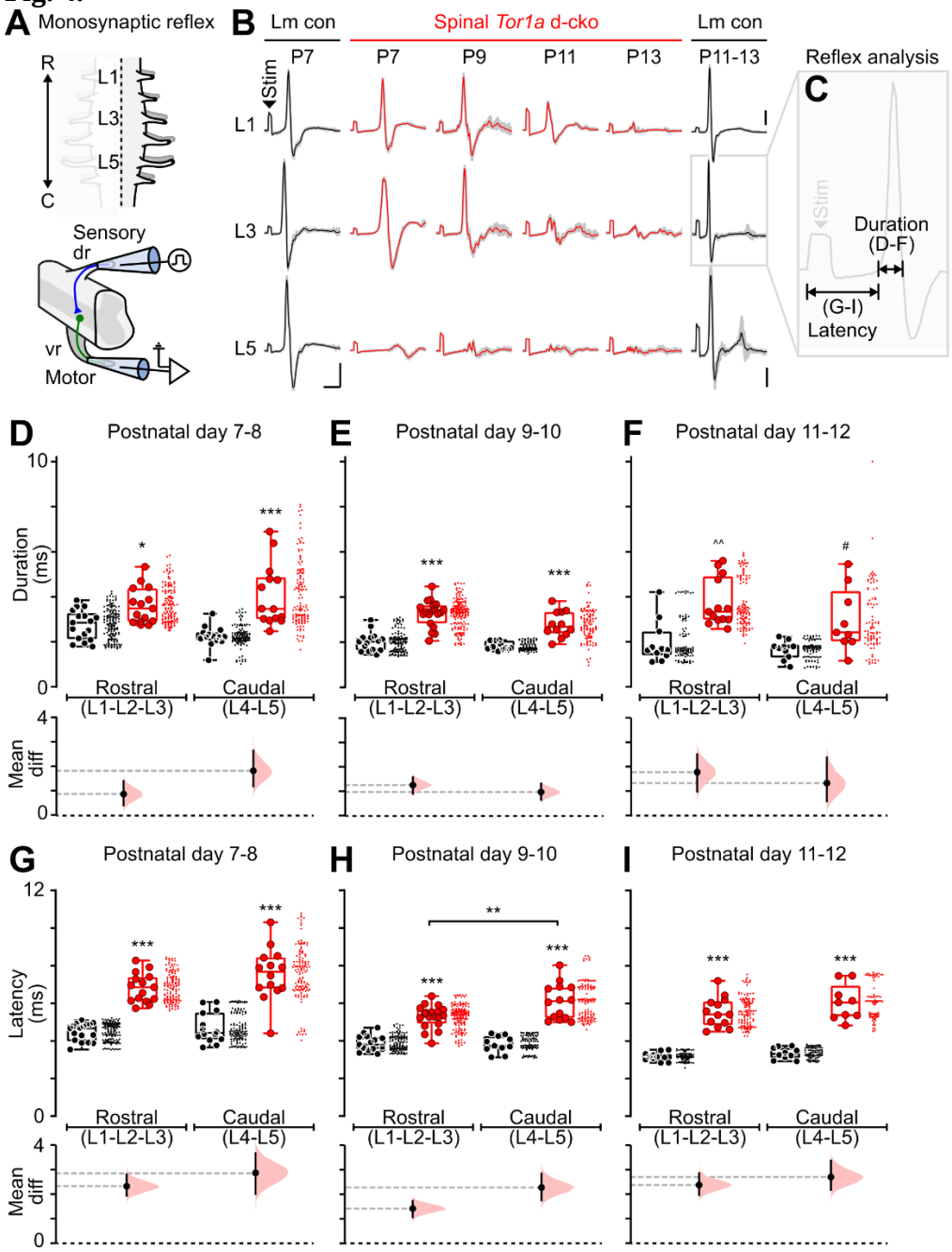

Fig. 4 Spinal-restricted *Tor1a* deletion impairs the monosynaptic reflex. (**A**) Experimental design. (**B**) Representative monosynaptic reflexes. Data shown are average (bold) overlaid onto *N*=10 sweeps (gray). Scale: x=5ms; y=0.05mV. (**C**) Reflex outcome measures. At all ages and roots tested, the monosynaptic (**D-F**) response duration and (**G-I**) latency to onset was increased

in spinal *Tor1a* d-cko (N=21) vs control (N=24). *P<0.05, **P<0.01, ***P<0.0001, two-way ANOVA and Tukey's *post hoc* t-test; ^^P<0.001, Mann-Whitney; #P<0.05, independent t-test with Welch's correction. Group data shown (box plots) with individual values overlaid (circles) and mean differences (estimation plots). Dots: all reflexes analysed/animal. Statistics details in Table S1.

Fig. 5.

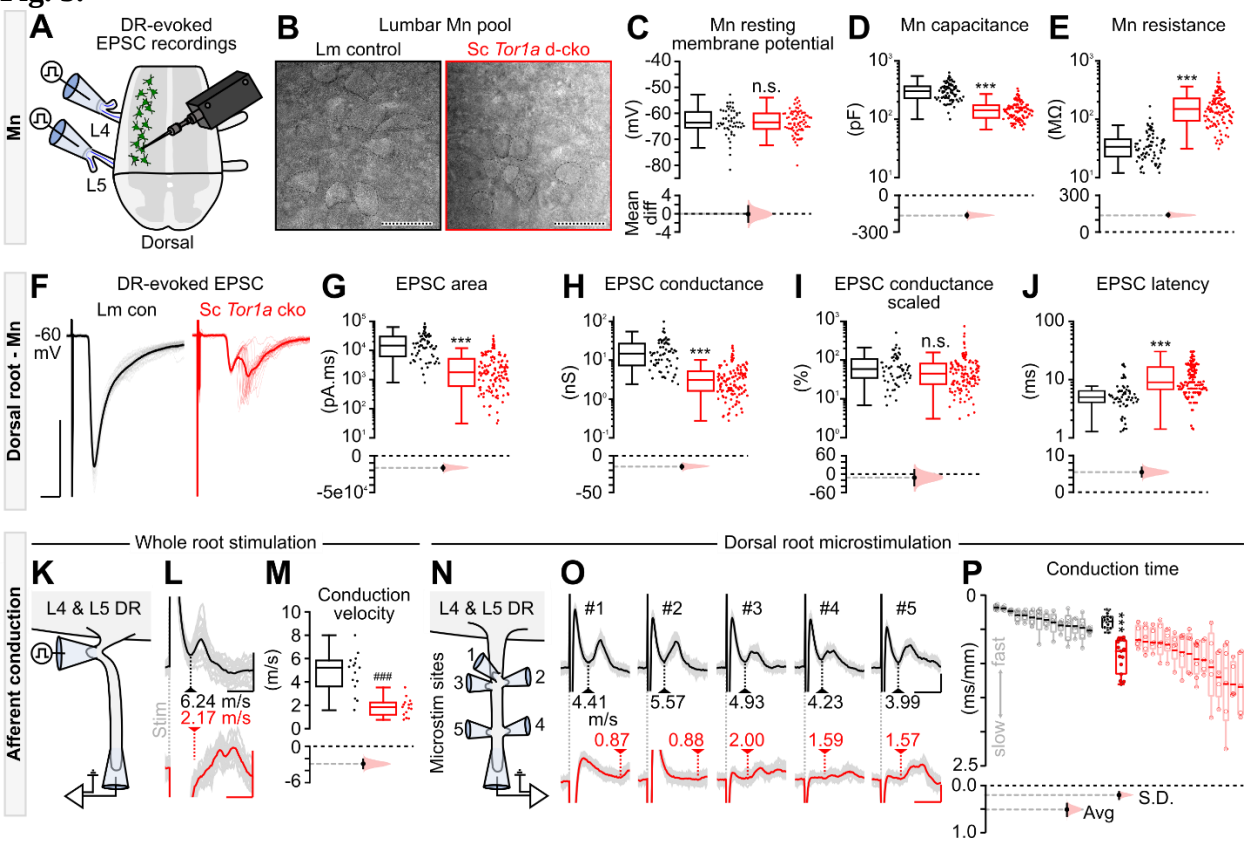

Fig. 5 All components of the monosynaptic reflex are impaired in spinal *Tor1a* d-cko mice (**A**) Experimental design to record afferent- and efferent-evoked excitatory post-synaptic potentials (EPSCs). (**B**) DIC images of P9 lumbar motoneurons (scale: 50µm). For intrinsic motoneuron properties (P1-P13 *N*=# of motoneurons), spinal *Tor1a* d-cko showed (**C**) no change in resting membrane potential (*N*=52 vs *N*=77, *P*=0.68, Mann-Whitney), (**D**) decreased whole cell capacitance (*N*=73 vs *N*=108, ***$P<0.0001$), and (**E**) increased input resistance (*N*=73 vs *N*=111). (**F**) P7 dorsal root (DR)-evoked EPSCs. Scale: x=5ms, y=500pA. Spinal *Tor1a* d-cko showed (**G**) decreased area (*N*=61 vs *N*=130), (**H**) decreased absolute conductance (*N*=61 vs *N*=128), (**I**) no change in scaled conductance (*N*=61 vs *N*=126, *P*=0.06), and (**J**) increased latency (*N*=60 vs *N*=131) (P1-P13). Group data shown (box plots) with mean differences (estimation plots). Dots: all responses analysed/animal. (**K**) DR stimulation to estimate afferent conduction velocity. (**L**)

Representative afferent volleys following whole root stimulation at threshold. Scales: x=0.5ms, y=0.05mV (black) or 0.025mV (red) (L5 DR in P8 control [n=20 sweeps] and P6 spinal *Tor1a* d-cko [n=35 sweeps]). (**M**) L4 & L5 DR conduction velocity is decreased in spinal *Tor1a* d-cko (P6-P10 N=15 vs N=15, $^{\#\#\#}P<0.0001$; independent t-test). (**N-O**) DR microstimulation revealed varied afferent conduction velocities in spinal *Tor1a* d-cko (black scale: x=0.5ms, y=0.05mV; red scale: x=3ms, y=0.025mV). (**P**) Spinal *Tor1a* d-cko afferent conduction time was slower (P6-P10, N=14 control vs N=15 cko, Avg: ***$P<0.0001$) and more variable (S.D.: ***$P<0.0001$). Averaged data shown in black and red box plots with individual values (means within each root) overlaid (filled circles) and mean differences (estimation plots). The responses from individual roots - including raw (open circles) and averaged (bold line) values - are shown as de-saturated box plots adjacent to the averaged dataset. Statistics details in Table S1.